Calculation of $(e, 2e)$ triple-differential cross sections of formic acid: An application of the multicenter distorted-wave method

Xingyu Li,[1,2,*] Maomao Gong,[1] Ling Liu,[2] Yong Wu,[2] Jianguo Wang,[2] Yizhi Qu,[3] and Xiangjun Chen[1,4,†]

[1]*Hefei National Laboratory for Physical Sciences at Microscale and Department of Modern Physics, University of Science and Technology of China, Hefei, Anhui 230026, China*

[2]*Data Center for High Energy Density Physics, Institute of Applied Physics and Computational Mathematics, Beijing 100088, China*

[3]*College of Material Sciences and Optoelectronic Technology, University of the Chinese Academy of Sciences, Beijing 100049, China*

[4]*Synergetic Innovation Center of Quantum Information and Quantum Physics, University of Science and Technology of China, Hefei, Anhui 230026, China*

(Received 29 June 2016; revised manuscript received 21 November 2016; published 17 January 2017)

The calculation of triple-differential cross sections for the electron-impact ionization of $10a'$ and $2a''$ orbitals of the formic acid (HCOOH) molecule has been carried out by the multicenter distorted-wave method. The coplanar asymmetric kinematics is considered at incident energies of 100 and 250 eV, where previous experiments and theories are available for comparison. The present calculations reproduce the experimental measurements satisfactorily and the results suggest that the nuclear distribution has important contributions on the cross sections at large momentum transfers.

DOI: 10.1103/PhysRevA.95.012703

I. INTRODUCTION

The probability of electron-impact single ionization is characterized by the triple-differential cross section (TDCS), which is sensitive to both the electronic structure of the target and the dynamics of the ionization process. It remains to be one of the biggest challenges to find a systematic theoretical description of TDCS for complex atomic and molecular systems, especially for the case of molecules, for which the anisotropic multicenter nature and the complexity of the electronic structure become big obstacles. The anisotropic nature, together with the fact that molecules are oriented randomly in experiments, forces one to do the spherical average in the calculation, and the complex molecular structure makes it hard to describe the interaction between the bound electrons and the free ones.

Different kinds of theoretical methods have been developed in the past years, including perturbative treatments, such as the distorted-wave impulse approximation [1], the distorted-wave Born approximation [2], and the Brauner-Briggs-Klar model [3,4], and nonperturbative treatments, such as the B-spline R-matrix approach [5], the time-dependent close-coupling (TDCC) method [6], the converged close-coupling (CCC) method [7], as well as the exterior complex scaling (ECS) method [8]. We note that the nonperturbative TDCC, CCC, and ECS methods have been applied to some simple diatomic molecules [9–15], but their extension to more complex molecular targets is very difficult. The main task for the perturbative methods is the modeling of the continuum electrons in the final channel of the ionized system, according to which we can separate those perturbative methods into two groups: one was built to treat small (two-center or three-center) molecules only, and the other was aimed to be general. In the first type, much attention was paid to include the multicenter nature in the continuum wave functions. For small molecules one would use either the effective approximation [16,17] or the production of continuum wave functions at each center [18–22]. For the simplest molecular ion, H_2^+, the prolate spherical coordinate method [23] provides an elaborate description for the real two-center continuum wave function. In the second type, in order to build a general method, Champion and coworkers [24–26] modeled the ejected electron as moving under the spherically averaged potential of the molecular ion. More elaborately, in their molecular three-body distorted-wave (M3DW) approximation, Madison and coworkers [27–33] solved the incident, scattered, and ejected continuum wave functions under the spherically averaged potentials, and in addition they introduced the orientation averaged molecular orbital (OAMO) approximation to cancel the anisotropic multicenter nature of the ionized molecular orbital. Recently Chaluvadi *et al.* [34] and Ali *et al.* [35] adopted the proper average method to the M3DW method. In the new approach, they spherically averaged the differential cross sections for all molecular orientations. Another approach based on the complex Kohn variational method was developed by Lin *et al.* [36,37], where the wave function of the ejected electron was solved by the close-coupling method.

Recently we have developed a general method [38], treating the electron-impact single ionization of molecules under asymmetric kinematics, where the energy of the scattered electron is much higher than the ejected one. While the incident and scattered electrons are described by plane waves due to the fact that they are fast, our multicenter distorted-wave (MCDW) method solves the motion for the ejected electron in the anisotropic potential of the molecular ion. Then a spherical average is taken after calculating differential cross sections for all molecular orientations. Former application to the water molecule showed a good agreement with the experimental measurements, thus validating the treatment for the ejected electron and underlying the importance of properly taking into account molecular orientation. Owing to the separate treatment of the bound electrons and continuum electron, the MCDW method can readily be applied to larger molecules.

*lixingyu@mail.ustc.edu.cn
†xjun@ustc.edu.cn

In the present paper, we focus on the study of the dynamics in $(e,2e)$ processes of the formic acid (HCOOH) molecule. Recently, Colyer *et al.* [39] measured the TDCSs of formic acid for the electron-impact ionization from its valence orbitals at 100- and 250-eV incident energies under coplanar asymmetric kinematics. In their paper, comparisons with the M3DW and M3DW with the Correlation-Polarization and Exchange-distortion potentials (M3DW-CPE) calculations were made, and there were significant discrepancies between the calculations and the measurements. In the present work, the MCDW calculations are carried out under the same kinematical arrangements. We compare the calculations where the nuclear term in the scattering potential is either fully included or approximated simply by the Coulomb tail. As will be shown later, the present MCDW calculations reproduce the experimental data more satisfactorily. The paper is organized as follows: in the next section, the theory of the MCDW method is briefly described. In Sec. III, discussions and comparisons are made. In the last section conclusions are presented.

Atomic units are used throughout the paper unless explicitly stated otherwise.

II. THEORETICAL METHOD

Since the details of the MCDW method have been given in [38], here we will only briefly outline its formulation. The MCDW method is developed within the framework of the first Born approximation (FBA), with special attention to the modeling of the continuum wave function of the ejected electron to include the anisotropic multicenter nature. Its main idea is to calculate differential cross sections for all molecular orientations and then do the average. This is applicable since the collision process is much faster than the rotation of molecules. In practice, the symmetry property of molecular targets is employed to simplify the calculation.

A. General formulation

In usual scattering theory, the wave function of the initial state of the $N+1$-electron system is the product of a bound molecular state wave function and a plane wave describing the incident electron. If the whole interaction between the incident electron and the molecular target is taken as the scattering potential, then within the FBA framework, the final state can also be written as a product of the wave function describing a molecule in the ionized state and a plane wave representing the scattered electron. The nonrelativistic eightfold-differential cross section for a given molecular orientation reads [40]

$$\frac{d^8\sigma}{d\Omega_e d\Omega_s d\Omega dE_s} = \frac{1}{(2\pi)^5}\frac{k_e k_s}{k_i}|T_{fi}(\Omega)|^2, \tag{1}$$

where Ω_s and Ω_e represent the solid angles of detections for the scattered and ejected electrons, respectively. The momenta $\boldsymbol{k}_i$, $\boldsymbol{k}_s$, and $\boldsymbol{k}_e$ are for the incoming, scattered, and ejected electrons, respectively. The molecular orientation is defined by Euler angle $\Omega=(\alpha,\beta,\gamma)$. The FBA transition amplitude in the laboratory reference reads

$$T_{fi}(\Omega) = \left\langle \boldsymbol{k}_s \Psi_f^{(-)}\left(\boldsymbol{k}_e;\mathcal{R}_\Omega^{-1}\{\boldsymbol{r}\}\right)|V|\boldsymbol{k}_i\Psi_i\left(\mathcal{R}_\Omega^{-1}\{\boldsymbol{r}\}\right)\right\rangle, \tag{2}$$

where the operator $\mathcal{R}_\Omega^{-1}$ represents the rotation of the target. $|\Psi_i\rangle$ is the initial bound wave function, and $\{\boldsymbol{r}\}$ refers to the set of electron coordinates. $|\Psi_f^{(-)}\rangle$ describes the ionized state of the molecule in the final channel. Furthermore, the incident and scattered electrons are described by plane waves $|\boldsymbol{k}_i\rangle$ and $|\boldsymbol{k}_s\rangle$. The scattering potential V includes the whole interaction between the incident electron and the molecular target:

$$V = \sum_e^N \frac{1}{|\boldsymbol{r}_e-\boldsymbol{r}_i|} - \sum_n \frac{Z_n}{|\boldsymbol{R}_n-\boldsymbol{r}_i|}, \tag{3}$$

where $\boldsymbol{R}_n$ is the position of the nth nucleus, and Z_n indicates its charge. The vectors $\boldsymbol{r}_e$ and $\boldsymbol{r}_i$ refer to the positions of the eth bound electron of the target and the incident electron, respectively.

With the help of the Bethe integral

$$\int \frac{e^{i\boldsymbol{k}\cdot\boldsymbol{r}'}}{|\boldsymbol{r}-\boldsymbol{r}'|}d\boldsymbol{r}' = \frac{4\pi}{k^2}e^{i\boldsymbol{k}\cdot\boldsymbol{r}}, \tag{4}$$

Eq. (2) can be simplified as

$$\begin{aligned} T_{fi}(\Omega) &= \frac{4\pi}{K^2}\left\langle \Psi_f^{(-)}\left(\boldsymbol{k}_e;\mathcal{R}_\Omega^{-1}\{\boldsymbol{r}\}\right)\right| \sum_e^N \left\{ e^{i\boldsymbol{K}\cdot\boldsymbol{r}_e} - \frac{\sum_n Z_n e^{i\boldsymbol{K}\cdot\boldsymbol{R}_n}}{N}\right\} \\ &\quad \times \left|\Psi_i\left(\mathcal{R}_\Omega^{-1}\{\boldsymbol{r}\}\right)\right\rangle, \end{aligned} \tag{5}$$

where $\boldsymbol{K}=\boldsymbol{k}_i-\boldsymbol{k}_s$ is the momentum transfer.

Under the frozen core approximation, the N-electron problem can be reduced to a one-active-electron problem, which gives rise to the following expression:

$$\begin{aligned} T_{fi}(\Omega) = \frac{4\pi}{K^2}\langle \mathcal{F}^{(-)}(\boldsymbol{k}_e;\mathcal{R}_\Omega^{-1}\boldsymbol{r})|e^{i\boldsymbol{K}\cdot\boldsymbol{r}_e} - \frac{\sum_n Z_n e^{i\boldsymbol{K}\cdot\boldsymbol{R}_n}}{N} \\ \times |\phi_\alpha(\mathcal{R}_\Omega^{-1}\boldsymbol{r})\rangle, \end{aligned} \tag{6}$$

where $|\mathcal{F}^{(-)}\rangle$ is the continuum wave function of the ejected electron, and $|\phi_\alpha\rangle$ is the wave function of the ionized bound orbital. The first term in Eq. (6) represents the scattering by the active electron, and the second term refers to the scattering by the nuclei. This nuclear term is dropped if one assumes the orthogonality between the initial bound and the final continuum states. However, in the present model, the ejected wave function is solved under the one-active-electron approximation, and is generally not orthogonal to the bound orbital $|\phi_\alpha\rangle$. In our previous study [38], we further assumed that the nuclei are localized within a small region, enabling us to substitute the nuclear term by 1, which is known as the Coulomb tail. In this case, the transition amplitude is approximated by

$$T_{fi}(\Omega) \approx \frac{4\pi}{K^2}\langle \mathcal{F}^{(-)}(\boldsymbol{k}_e;\mathcal{R}_\Omega^{-1}\boldsymbol{r})|e^{i\boldsymbol{K}\cdot\boldsymbol{r}_e}-1|\phi_\alpha(\mathcal{R}_\Omega^{-1}\boldsymbol{r})\rangle. \tag{7}$$

This approximation was applied for the water molecule in our previous study [38], and it was reasonable since both the mass and nuclear charge concentrate mainly on the O atom. However, it is not the case for the formic acid molecule, which is composed of more atoms, and the distributions of which of the mass and nuclear charge are more dispersive. In the present paper, the calculations are carried out employing both models,

where the nuclear term is either approximated by the Coulomb tail (MCDW) or fully included (MCDW-NT).

Finally, the fivefold differential cross section, or the commonly termed TDCS, is obtained by averaging over all possible molecular orientations:

$$\frac{d^5\sigma}{d\Omega_e d\Omega_s dE_s} = \frac{1}{(2\pi)^5}\frac{k_e k_s}{k_i}\frac{1}{8\pi^2}\int |T_{fi}(\Omega)|^2\, d\Omega. \quad (8)$$

B. Multicenter distorted wave

In the single ionization process, one bound electron is excited to continuum orbitals, which have no preferable orientation. However, in the experiment we detect electrons with a specific momentum, thus a linear combination of all possible continuum orbitals must be applied to produce a wave function corresponding to that specific momentum.

It is formidable to solve this continuum wave function exactly, and we will limit ourselves to the single-active-electron approximation instead: the ejected electron is regarded as moving in the anisotropic field of the molecular ion, while the scattered electron is too fast to affect its motion. To include the response of the bound electrons in the ion and the exchange effect, a model potential is adopted [41]:

$$V^{\rm m} = V^{\rm st} + V^{\rm cp} + V^{\rm model\ exc}, \quad (9)$$

where $V^{\rm st}$ includes the static potentials between the incident electron and the electrons and nuclei in the residual molecular ion. $V^{\rm cp}$ and $V^{\rm model\ exc}$ are the correlation-polarization potential and the model exchange potential, respectively.

The Schrödinger equation with the model potential is

$$\left[-\tfrac{1}{2}\nabla^2 + V^{\rm m} - E_{k_e}\right]\mathcal{F}^{(-)}(\boldsymbol{k}_e;\boldsymbol{r}) = 0, \quad (10)$$

where $\mathcal{F}^{(-)}(\boldsymbol{k}_e;\boldsymbol{r})$ indicates the continuum wave function of the ejected electron. Clearly the anisotropic multicenter nature of $\mathcal{F}^{(-)}(\boldsymbol{k}_e;\boldsymbol{r})$ is inherited from $V^{\rm m}$. To solve the model Schrödinger equation, the single-center expansion technique [41–43] is employed, where the wave function and potential are expanded over symmetry-adapted angular functions. Note that the anisotropy of the model potential $V^{\rm m}$ will cause the coupling between terms of different angular momenta, resulting in a set of radial coupled equations. As in our previous work [38], the diagonal terms in the potential matrix are considered dominant. Thus in practice, we will ignore the off-diagonal elements and solve the decoupled partial wave equations. For the calculation details, one can refer to Ref. [38].

III. RESULTS AND DISCUSSION

The formic acid molecule belongs to the Cs symmetry point group, and its ground-state configuration is $(\text{core})^6 4a'^2 5a'^2 6a'^2 7a'^2 8a'^2 1a''^2 9a'^2 2a''^2 10a'^2$. In the present paper, we will consider the ionization of its two outermost molecular orbitals (MOs) $10a'$ and $2a''$, for which experimental data are available in Ref. [39]. The orbital maps of the two MOs are illustrated in Fig. 1, showing that $10a'$ is of sp type and $2a''$ is of p type.

The experiments of Colyer *et al.* [39] were performed under coplanar asymmetric kinematics for two incident energies of 100 and 250 eV. In both cases the ejected electron energy was chosen to be 10 eV. The TDCSs for $E_i = 100$ eV were measured at scattering angles (θ_s) of -10 and -15°, and the TDCSs for $E_i = 250$ eV were measured at $\theta_s = -5, -10$, and -15°. According to Colyer *et al.* [39] the binding energies for $10a'$ and $2a''$ are 11.6 and 12.5 eV, respectively. The coincidence energy resolution of their work is approximately 1.2 eV in FWHM, thus the two orbitals cannot be resolved. We need to sum over the individual TDCSs of the two orbitals to produce data comparable to the measurements.

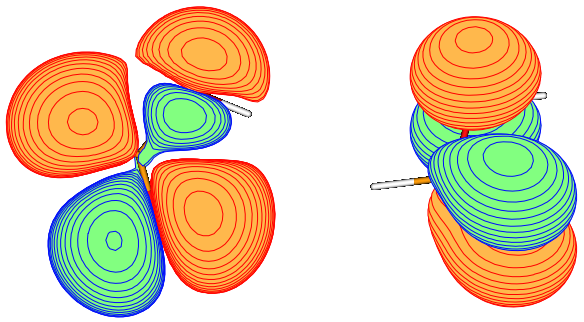

FIG. 1. Illustrations of molecular orbital $10a'$ (left) and $2a''$ (right).

In our calculation, the geometry of formic acid is optimized and the wave functions of the MOs are calculated using the GAUSSIAN 03W [44] program with the density functional theory method employing B3LYP hybrid functional [45,46] and the DGauss triple zeta valence polarized basis set [47]. Then the MOs are expanded into the symmetry-adapted angular functions. Let $l^b_{\rm max}$ and $l^c_{\rm max}$ denote the upper limits of angular momentum in the partial wave expansions for the bound orbital and continuum wave function, respectively. Convergence is achieved in our calculation with $l^b_{\rm max} = 10$ and $l^c_{\rm max} = 18$. In the single-center expansion, the r ranges from 0 to 8.47 a.u. with increasing step size from 0.01 to 0.128 a.u. The numerical spherical average reaches its convergence with the Euler angle mesh $N_\alpha = N_\beta = N_\gamma = 16$, where N_α, N_β, and N_γ denote the number of points for Euler angle α, β, and γ, respectively.

Figure 2 shows the results of summed TDCSs of $10a'$ and $2a''$ orbitals at the incident energy of 100 eV. Both the MCDW-NT and MCDW calculations are included and compared with the experimental data and the calculations by the M3DW and M3DW-CPE method [39]. The measurements are visually normalized to the binary peaks of the MCDW-NT calculations, while the M3DW and M3DW-CPE results are kept in absolute scale as in Ref. [39]. It should be noted that the M3DW calculations are based on the OAMO approximation, which is not valid for the $2a''$ orbital since the average is zero for this symmetry (as shown in Fig. 1). Meanwhile, the $10a'$ orbital is also partially canceled due to the orientation average. Consequently, only the results for the $10a'$ orbital are valid in the M3DW and M3DW-CPE calculations. For both scattering angles, our results show broad binary peaks and broad recoil peaks with no finer structure. The MCDW and MCDW-NT calculations reproduce the experiments reasonably, especially for the binary peaks. For the recoil peaks, the MCDW calculations reproduce the experiments well, while the MCDW-NT calculations predict lower intensities. On the other hand, the M3DW and M3DW-CPE calculations both produce sharp and intense binary peaks. This is the consequence of the

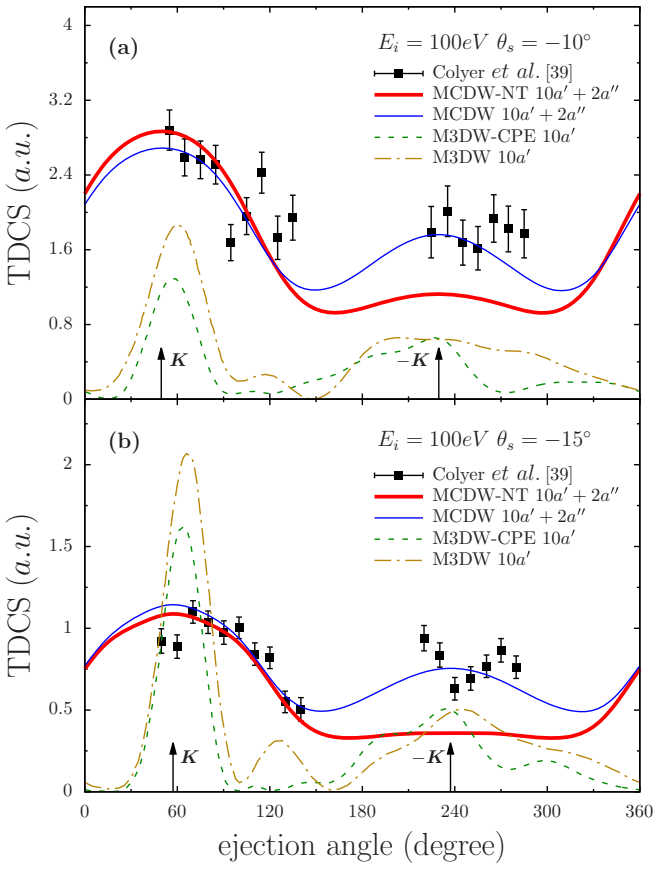

FIG. 2. The summed TDCSs for $10a'$ and $2a''$ orbitals at incident energy of 100 eV and ejected energy of 10 eV. Both the MCDW-NT calculations (thick red solid lines) and the MCDW calculations (blue solid lines) are included. Comparisons are made with the experimental data (solid square), the M3DW (dark yellow dash-dotted lines), and M3DW-CPE (dark green dashed lines) calculations. The scattering angles and the corresponding magnitudes of the momentum transfers are (a) $-10°$, $|\boldsymbol{K}| = 0.55$ a.u. and (b) $-15°$, $|\boldsymbol{K}| = 0.74$ a.u.

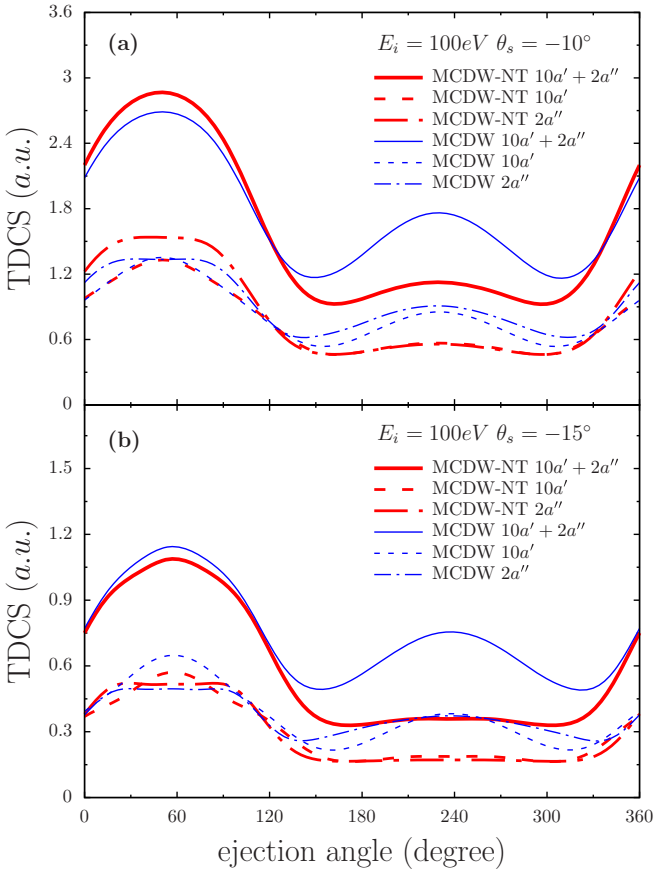

FIG. 3. Individual and summed TDCSs for $10a'$ and $2a''$ orbitals at incident energy of 100 eV and ejected energy of 10 eV. The thick red lines refer to the MCDW-NT calculations: summed TDCSs (thick solid lines), TDCSs for $10a'$ orbital (thick dashed lines), and TDCSs for $2a''$ orbital (thick dash-dotted lines). The blue lines refer to the MCDW calculations: summed TDCSs (solid lines), TDCSs for $10a'$ orbital (dashed lines), and TDCSs for $2a''$ orbital (dash-dotted lines). The scattering angles and the corresponding magnitudes of the momentum transfers are (a) $-10°$, $|\boldsymbol{K}| = 0.55$ a.u. and (b) $-15°$, $|\boldsymbol{K}| = 0.74$ a.u.

OAMO approximation, which transforms the $10a'$ orbital into a spherically symmetric atomiclike effective orbital.

In order to have better insight into the characters of the $(e,2e)$ process, it is worthwhile to investigate the individual TDCSs for each orbital. In Fig. 3 the TDCSs for $10a'$ and $2a''$ orbitals and their sum, calculated by the MCDW-NT and MCDW methods, are presented. In principle, under coplanar asymmetric kinematics, the binary peak contains a strong signature of the orbital shape. For the atomic s orbital, there should be a single peak along the direction of momentum transfer, while for the atomic p orbital the binary peak should split into two. For the $10a'$ orbital, both s-type and p-type features are involved, producing a broad peak with a sharp top. For the p-type $2a''$ orbital, a double-peak structure is expected. However, the distortion on the ejected electron from the molecular ion makes it a flat top at both scattering angles. It is clear that the broadness of the binary peaks is the result of a p-type component that is contained in both orbitals.

In Fig. 4, we present the summed TDCSs of $10a'$ and $2a''$ orbitals by the MCDW-NT and MCDW calculations at the incident energy of 250 eV and the ejected energy of 10 eV for the three scattering angles of -5, -10, and $-15°$. The experimental data and the results of the M3DW and M3DW-CPE calculations [39] are also plotted in the figure for comparison. The normalization procedure is similar to that adopted in Fig. 2. At this incident energy, the MCDW-NT calculations reproduce the measurements to a reasonable level, while the MCDW calculations overestimate the experiments at the scattering angle of $-15°$. At $\theta_s = -5$ and $-15°$, the binary peaks of our calculations shift to the lower ejection angle by about 10–15° with respect to the experiment data. The shape of the measured binary peak at the scattering angle of $-15°$ is considerably different from the other two. Both the MCDW-NT and MCDW results reproduce such difference, presenting one sharp peak at the center with two shoulders at both sides. It is worthy to note that our MCDW-NT calculations successfully reproduce the rapid decrease of the intensity of the recoil peaks with increasing scattering angle. In fact, at $\theta_s = -15°$, there is a valley rather than a peak in the recoil

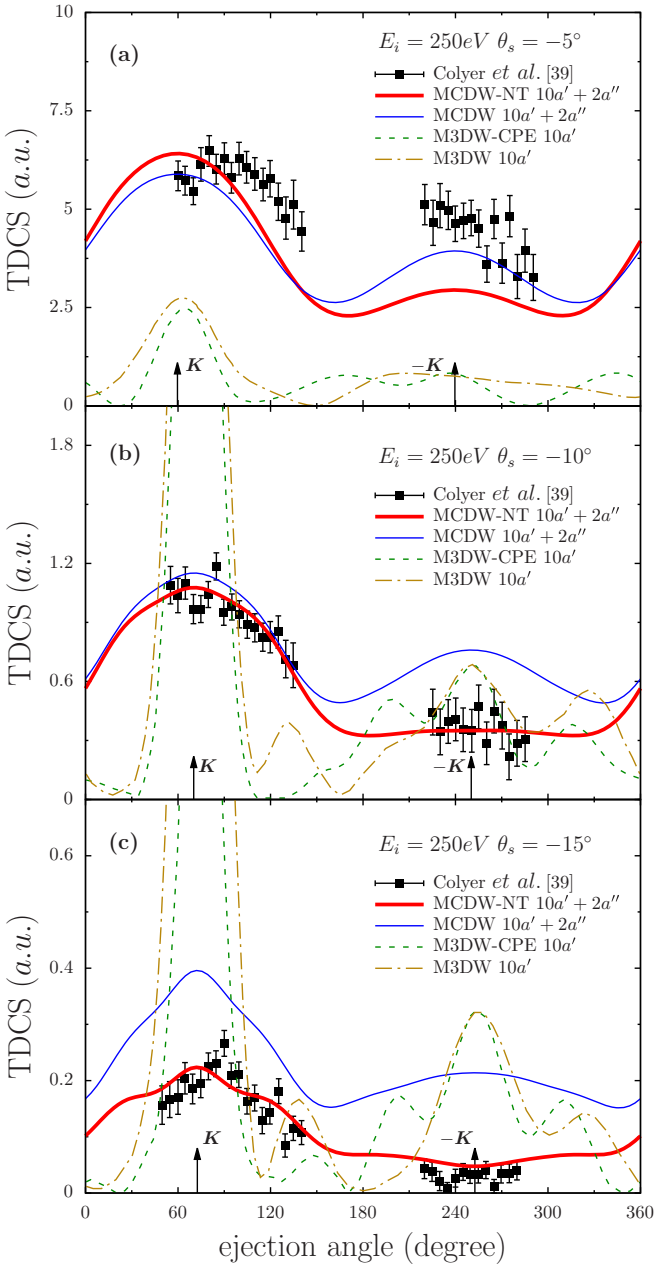

FIG. 4. Same as in Fig. 2 but at incident energy 250 eV. The scattering angles and the magnitudes of corresponding momentum transfers are (a) $-5°$, $|\boldsymbol{K}| = 0.41$ a.u., (b) $-10°$, $|\boldsymbol{K}| = 0.76$ a.u., and (c) $-15°$, $|\boldsymbol{K}| = 1.11$ a.u.

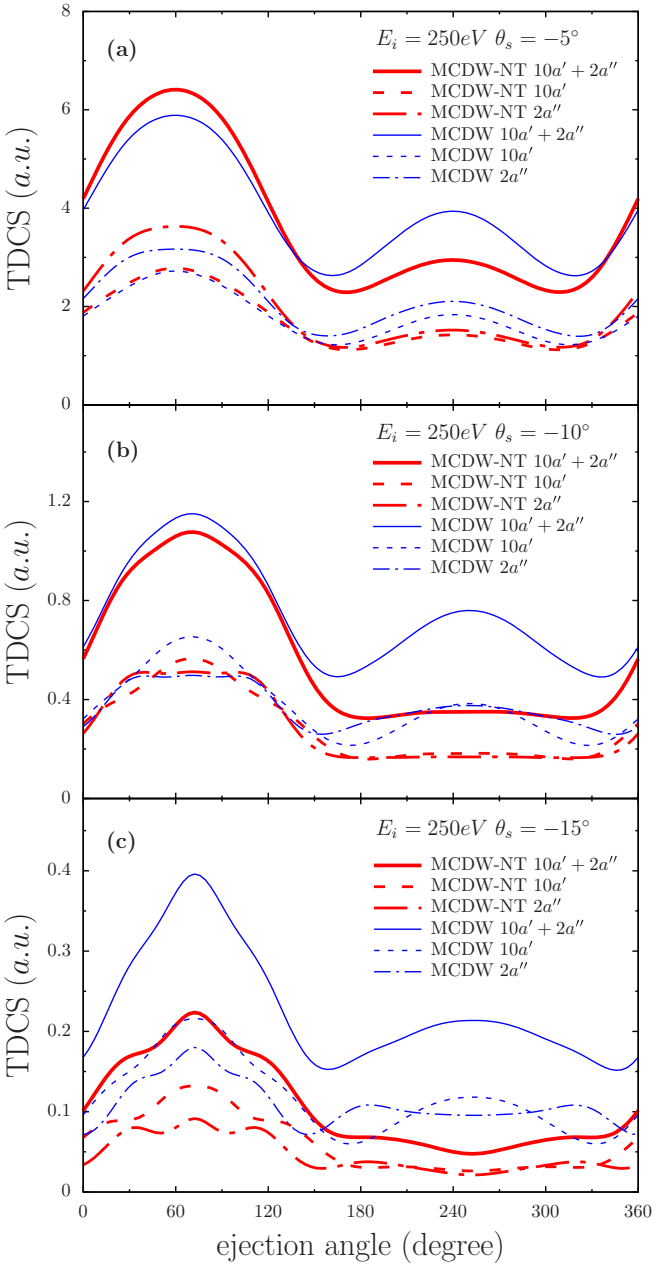

FIG. 5. Same as in Fig. 3 but at incident energy 250 eV. The scattering angles and the magnitudes of corresponding momentum transfers are (a) $-5°$, $|\boldsymbol{K}| = 0.41$ a.u., (b) $-10°$, $|\boldsymbol{K}| = 0.76$ a.u., and (c) $-15°$, $|\boldsymbol{K}| = 1.11$ a.u.

region. This suggests the importance of considering the nuclear distribution in the scattering potential.

The summed and individual TDCSs of the MCDW-NT and MCDW calculations for $10a'$ and $2a''$ orbitals at $E_i = 250$ eV are presented in Fig. 5. It can be found that the features of the results at scattering angles of -5 and $-10°$ are similar to those at $\theta_s = -10$ and $-15°$ in Fig. 3, respectively. This is due to the fact that the magnitudes of momentum transfers in the corresponding cases are similar. From the individual TDCSs we find two facts accounting for the rapid change in the binary peak shape: First, the TDCS for the $10a'$ orbital gradually surpasses the one for the $2a''$ orbital as the scattering angle increases. The same tendency can be found for the $E_i = 100$ eV case. Second, at the scattering angles of -10 and $-15°$, a small peak appears in addition to the flat structure at the center of the binary peak of the $2a''$ orbital. It becomes more significant with increasing scattering angle. The second feature may be due to the distortion effect: the bigger the scattering angle is, the closer the incident electron reaches the inner region of the target, and as the ejected electron is kicked out, it suffers more distortion from the residual ion. Finally, we note that there are additional structures in the individual TDCSs at the scattering angle of $-15°$. The MCDW-NT calculations predict an oscillatory structure with

flat minimum around 250° in the recoil region for the TDCSs of both orbitals, while the $10a'$ TDCS of the MCDW calculations shows a maximum which is slightly dominant. This results in summed TDCSs, which are different for the MCDW-NT and MCDW calculations in the recoil region.

IV. CONCLUSION

The multicenter distorted-wave method has been applied in calculating the TDCSs of $(e,2e)$ processes of formic acid at the incident energies of 100 and 250 eV under coplanar asymmetric kinematics. The results are compared with the measurements of Colyer *et al.* [39] and the M3DW and M3DW-CPE calculations provided by the same authors. In the present work, both the MCDW-NT and MCDW calculations are performed, where the nuclear term in the scattering potential is fully included in the former and simply approximated by the Coulomb tail in the latter. At the incident energy of 250 eV, the MCDW-NT calculations reproduce the measurements reasonably in both binary and recoil regions for all three scattering angles, while at the lower incident energy of 100 eV it predicts lower recoil peak intensities. This is to be expected since the multicenter distorted-wave method is built within the FBA framework and should be more legitimate for higher incident energy. On the other hand, the MCDW calculations reproduce the measurements at lower incident energy of 100 eV, but the agreement become poorer at $E_i = 250$ eV. Its agreement at lower incident energy is more likely to be a coincidence. And the failure of the MCDW-NT calculations in describing the recoil peaks at $E_i = 100$ eV is probably due to the approximations made in our method, i.e., ignoring the off-diagonal terms and the lack of orthogonality, and high-order effects beyond the FBA.

Based on our calculations, the main features of the TDCSs can be explained. The broad binary peaks reflect the contributions from p-type components in both $10a'$ and $2a''$ orbitals. The significant change in the binary peak shape as the scattering angle varies is a result of the intensities' behavior of individual TDCSs, as well as the distortion effect on the ejected electron. However, the angular range of the ejected electron and the data statistics in the experiments are quite limited, preventing us from having a thorough understanding of the dynamics. New experiments are highly desired for further study.

ACKNOWLEDGMENT

This work was supported by the National Natural Science Foundation of China (Grants No. 11534011 and No. 11327404).

[1] I. McCarthy and E. Weigold, Phys. Rep. **27**, 275 (1976).
[2] D. H. Madison, R. V. Calhoun, and W. N. Shelton, Phys. Rev. A **16**, 552 (1977).
[3] C. R. Garibotti and J. E. Miraglia, Phys. Rev. A **21**, 572 (1980).
[4] M. Brauner, J. S. Briggs, and H. Klar, J. Phys. B **22**, 2265 (1989).
[5] O. Zatsarinny and K. Bartschat, Phys. Rev. Lett. **107**, 023203 (2011).
[6] M. S. Pindzola, F. Robicheaux, S. D. Loch, J. C. Berengut, T. Topcu, J. Colgan, M. Foster, D. C. Griffin, C. P. Ballance, D. R. Schultz, T. Minami, N. R. Badnell, M. C. Witthoeft, D. R. Plante, D. M. Mitnik, J. A. Ludlow, and U. Kleiman, J. Phys. B **40**, R39 (2007).
[7] I. Bray and A. T. Stelbovics, Phys. Rev. A **46**, 6995 (1992).
[8] C. W. McCurdy and T. N. Rescigno, Phys. Rev. A **56**, R4369 (1997).
[9] J. Colgan, M. S. Pindzola, F. Robicheaux, C. Kaiser, A. J. Murray, and D. H. Madison, Phys. Rev. Lett. **101**, 233201 (2008).
[10] J. Colgan, O. Al-Hagan, D. H. Madison, C. Kaiser, A. J. Murray, and M. S. Pindzola, Phys. Rev. A **79**, 052704 (2009).
[11] M. S. Pindzola, F. Robicheaux, and J. Colgan, J. Phys. B **38**, L285 (2005).
[12] M. S. Pindzola, F. Robicheaux, S. D. Loch, and J. P. Colgan, Phys. Rev. A **73**, 052706 (2006).
[13] M. S. Pindzola, S. A. Abdel-Naby, J. A. Ludlow, F. Robicheaux, and J. Colgan, Phys. Rev. A **85**, 012704 (2012).
[14] M. C. Zammit, D. V. Fursa, and I. Bray, Phys. Rev. A **87**, 020701 (2013).
[15] V. V. Serov and B. B. Joulakian, Phys. Rev. A **80**, 062713 (2009).
[16] P. F. Weck, O. A. Fojón, J. Hanssen, B. B. Joulakian, and R. D. Rivarola, Phys. Rev. A **63**, 042709 (2001).
[17] C. R. Stia, O. A. Fojón, P. F. Weck, J. Hanssen, B. Joulakian, and R. D. Rivarola, Phys. Rev. A **66**, 052709 (2002).
[18] P. F. Weck, O. A. Fojón, B. B. Joulakian, C. R. Stia, J. Hanssen, and R. D. Rivarola, Phys. Rev. A **66**, 012711 (2002).
[19] B. B. Joulakian, J. Hanssen, R. Rivarola, and A. Motassim, Phys. Rev. A **54**, 1473 (1996).
[20] O. Chuluunbaatar, B. B. Joulakian, K. Tsookhuu, and S. I. Vinitsky, J. Phys. B **37**, 2607 (2004).
[21] O. Chuluunbaatar and B. B. Joulakian, J. Phys. B **43**, 155201 (2010).
[22] O. Alwan, O. Chuluunbaatar, X. Assfeld, A. Naja, and B. B. Joulakian, J. Phys. B **47**, 225201 (2014).
[23] V. V. Serov, B. B. Joulakian, D. V. Pavlov, I. V. Puzynin, and S. I. Vinitsky, Phys. Rev. A **65**, 062708 (2002).
[24] C. Champion, J. Hanssen, and P. A. Hervieux, J. Chem. Phys. **117**, 197 (2002).
[25] C. Champion, J. Hanssen, and P. A. Hervieux, Phys. Rev. A **65**, 022710 (2002).
[26] C. Champion, C. Dal Cappello, S. Houamer, and A. Mansouri, Phys. Rev. A **73**, 012717 (2006).
[27] D. H. Madison and O. Al-Hagan, J. At. Mol. Opt. Phys. **2010**, 1 (2010).
[28] J. Gao, J. L. Peacher, and D. H. Madison, J. Chem. Phys. **123**, 204302 (2005).
[29] J. Gao, D. H. Madison, and J. L. Peacher, J. Chem. Phys. **123**, 204314 (2005).
[30] J. Gao, D. H. Madison, and J. L. Peacher, Phys. Rev. A **72**, 020701 (2005).

[31] J. Gao, D. H. Madison, and J. L. Peacher, Phys. Rev. A **72**, 032721 (2005).
[32] J. Gao, D. H. Madison, J. L. Peacher, A. J. Murray, and M. J. Hussey, J. Chem. Phys. **124**, 194306 (2006).
[33] J. Gao, D. H. Madison, and J. L. Peacher, J. Phys. B **39**, 1275 (2006).
[34] H. Chaluvadi, C. G. Ning, and D. Madison, Phys. Rev. A **89**, 062712 (2014).
[35] E. Ali, K. Nixon, A. J. Murray, C. Ning, J. Colgan, and D. H. Madison, Phys. Rev. A **92**, 042711 (2015).
[36] C.-Y. Lin, C. W. McCurdy, and T. N. Rescigno, Phys. Rev. A **89**, 012703 (2014).
[37] C.-Y. Lin, C. W. McCurdy, and T. N. Rescigno, Phys. Rev. A **89**, 052718 (2014).
[38] S. b. Zhang, X. Y. Li, J. G. Wang, Y. Z. Qu, and X. Chen, Phys. Rev. A **89**, 052711 (2014).
[39] C. J. Colyer, M. A. Stevenson, O. Al-Hagan, D. H. Madison, C. Ning, and B. Lohmann, J. Phys. B **42**, 235207 (2009).
[40] E. Weigold and I. E. McCarthy, *Electron Momentum Spectroscopy* (Springer, Boston, 1999).
[41] N. Sanna and F. Gianturco, Comput. Phys. Commun. **128**, 139 (2000).
[42] N. Sanna and G. Morelli, Comput. Phys. Commun. **162**, 51 (2004).
[43] N. Sanna, I. Baccarelli, and G. Morelli, Comput. Phys. Commun. **180**, 2544 (2009).
[44] M. J. Frisch, G. W. Trucks, H. B. Schlegel, G. E. Scuseria, M. A. Robb, J. R. Cheeseman, J. A. Montgomery Jr., T. Vreven, K. N. Kudin, J. C. Burant, J. M. Millam, S. S. Iyengar, J. Tomasi, V. Barone, B. Mennucci, M. Cossi, G. Scalmani, N. Rega, G. A. Petersson, H. Nakatsuji, M. Hada, M. Ehara, K. Toyota, R. Fukuda, J. Hasegawa, M. Ishida, T. Nakajima, Y. Honda, O. Kitao, H. Nakai, M. Klene, X. Li, J. E. Knox, H. P. Hratchian, J. B. Cross, V. Bakken, C. Adamo, J. Jaramillo, R. Gomperts, R. E. Stratmann, O. Yazyev, A. J. Austin, R. Cammi, C. Pomelli, J. W. Ochterski, P. Y. Ayala, K. Morokuma, G. A. Voth, P. Salvador, J. J. Dannenberg, V. G. Zakrzewski, S. Dapprich, A. D. Daniels, M. C. Strain, O. Farkas, D. K. Malick, A. D. Rabuck, K. Raghavachari, J. B. Foresman, J. V. Ortiz, Q. Cui, A. G. Baboul, S. Clifford, J. Cioslowski, B. B. Stefanov, G. Liu, A. Liashenko, P. Piskorz, I. Komaromi, R. L. Martin, D. J. Fox, T. Keith, M. A. Al-Laham, C. Y. Peng, A. Nanayakkara, M. Challacombe, P. M. W. Gill, B. Johnson, W. Chen, M. W. Wong, C. Gonzalez, and J. A. Pople, Gaussian 03, Revision C.02, Technical Report.
[45] A. D. Becke, J. Chem. Phys. **98**, 5648 (1993).
[46] C. Lee, W. Yang, and R. G. Parr, Phys. Rev. B **37**, 785 (1988).
[47] N. Godbout, D. R. Salahub, J. Andzelm, and E. Wimmer, Can. J. Chem. **70**, 560 (1992).